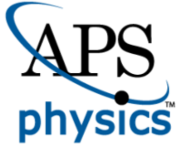

CHORUS

This is the accepted manuscript made available via CHORUS. The article has been published as:

Electrical Tuning of Exciton Binding Energies in Monolayer WS_{2}

Alexey Chernikov, Arend M. van der Zande, Heather M. Hill, Albert F. Rigosi, Ajanth Velauthapillai, James Hone, and Tony F. Heinz

Phys. Rev. Lett. **115**, 126802 — Published 16 September 2015

DOI: 10.1103/PhysRevLett.115.126802

Electrical tuning of exciton binding energies in monolayer WS_2

Alexey Chernikov†,[1] Arend M. van der Zande†,[1,2,3] Heather M. Hill,[1] Albert F. Rigosi,[1] Ajanth Velauthapillai,[1,4] James Hone,[2] and Tony F. Heinz[1,5,6]

[1] *Departments of Physics and Electrical Engineering, Columbia University, New York, NY 10027, USA*
[2] *Department of Mechanical Engineering, Columbia University, New York, New York 10027, USA*
[3] *Department of Mechanical Science and Engineering, University of Illinois at Urbana-Champaign, Urbana, IL 61801, USA*
[4] *Department of Physics and Materials Sciences Center, Philipps-Universität Marburg, Marburg, 35032, Germany*
[5] *Department of Applied Physics, Stanford University, Stanford, CA 94305, USA*
[6] *SLAC National Accelerator Laboratory, Menlo Park, CA 94025, USA*
† *These authors contributed equally to this work*

We demonstrate continuous tuning of the exciton binding energy in monolayer WS_2 by means of an externally applied voltage in a field-effect transistor device. Using optical spectroscopy, we monitor the ground and excited excitonic states as function of gate voltage and track the evolution of the quasi-particle band gap. The observed decrease of the exciton binding energy over the range of about 100 meV, accompanied by the renormalization of the quasi-particle band gap, is associated with screening of the Coulomb interaction by the electrically injected free charge carriers at densities up to $8{\cdot}10^{12}\,\mathrm{cm}^{-2}$. Complete ionization of the excitons due to the electrical doping is estimated to occur at a carrier density of several $10^{13}\,\mathrm{cm}^{-2}$.

A common feature of nanoscale materials is the presence of strongly enhanced Coulomb interactions between the charge carriers due quantum confinement effects and reduced dielectric screening. The resulting formation of tightly bound electron-hole pairs, or excitons, leads to a variety of intriguing phenomena, such as multiple exciton generation and the creation of excitonic molecules and complexes, as well as of exciton-polariton condensates. These many-body effects are significant both for the fundamental understanding of the materials and for their use in device applications. As important as the properties of the unperturbed system is the ability to tune excitonic states using external control. In this regard, the new class of semiconducting monolayer transition metal dichalcogenides (TMDCs) [1–3] shows much promise [4, 5]. In single- and few-layered TMDCs, the carriers can form strongly bound excitons [6–10], charged excitons [11, 12], and excitonic molecules [13]. The excitons exhibit binding energies of many 100's of meV [6–10, 14–25], strong inter- and intraband light-matter coupling [22, 26–28], efficient luminescence [2, 3, 29–31], and intriguing spin-valley physics [32–38]. Recent studies have also reported the manipulation of the ground-state transition energy in monolayer TMDCs using a variety of approaches [26, 39–43]. In contrast, external control of the exciton binding energy has not yet been demonstrated. This capability is, however, of great importance, since the optical and opto-electronic properties of the TMDC materials are strongly influenced by the large binding energies of the excitonic particles. In addition, from the practical point of view, semiconductor devices such as transistors, modulators, and emitters are operated using externally applied fields and at finite carrier densities. A detailed understanding of the material's properties under such conditions is thus crucial for the implementation of atomically thin TMDCs in future devices.

In this work, we demonstrate continuous, electrical tuning of the excitonic states in an electrostatically gated WS_2 monolayer. By measuring the energies of excited states of the band-edge exciton, known as the Rydberg series, we track the evolution of the exciton binding energies and the position of the quasi-particle band gap with gate voltage. We show that by changing the gate voltage in the FET device from -50 V to +50 V both the exciton binding energy and the quasi-particle band-gap energy can be tuned over a range of about 100 meV. The observed phenomena are attributed to the electrical injection (doping) of free charge carriers into the WS_2 monolayer and the resulting decrease of the exciton binding energies from screening of the Coulomb interaction. Our findings further allow us to identify a regime where complete ionization of the excitonic states occurs for electron densities of several $10^{13}\,\mathrm{cm}^{-2}$.

Monolayer WS_2 was obtained by mechanical exfoliation onto a 285-nm thick silicon dioxide thin film on a degenerately doped silicon wafer. The electron density is controlled by fabricating electrical contacts with electron beam lithography and utilizing the silicon substrate as a back gate. The optical properties of the exciton states are studied at different gate voltages by measuring the linear reflectance contrast $\Delta R/R = (R_{\mathrm{sample}} - R_{\mathrm{substrate}})/R_{\mathrm{substrate}}$ of the sample in vacuum at a temperature of 50 K. All material processing was performed at moderate temperatures ($< 130^o$C) to avoid possible sample degradation. Additional experimental details are given in the Supplemental Material [44].

Before examining the evolution of the higher states, we need to quantify the doping of the sample. We extract this information from the back gate capacitance and from the evolution of the ground state exciton. Figure 1 (a) shows the reflectance contrast in a color plot over the spectral range of the ground-state transition at different gate voltages V_g, while the individual $\Delta R/R$ spectra are presented in Fig. 1 (b) for selected voltages. At negative gate voltages, the spectrum is dominated by the neutral exciton resonance (X_0) originating from the so-called A-transition at the K and K' points of the Brillouin zone. As the gate voltage increases, an additional peak emerges at lower energies, and the X_0 resonance broadens and decreases in strength. The second feature is attributed to the negatively charged exciton, or trion (X-), which is composed of an exciton and an additional electron, and is typically observed in monolayer TMDCs at finite doping densities [11, 12, 36, 53–55]. We infer that the charge neutrality point of the sample is around $V_g = -45$ V; we then estimate the electron density in the monolayer from the capacitance of the back gate to increase to about $8(\pm1)\cdot10^{12}$ electrons cm^{-2} at the highest gate voltage of $V_g = 50$ V. The doping is consistent with the evolution of the energy difference between the exciton and trion resonances, proportional to the chemical potential of the electrons [11]. Additional information with respect to the doping conditions, gate-dependent photoluminescence, and room-temperature response is given in the Supplemental Material [44].

The experimental conditions in our study are further illustrated in Fig. 1(c), where the band structure of the WS_2 monolayer is shown schematically around the fundamental gap of the material. The conduction bands in WS_2 are predicted to exhibit a finite spin-splitting ΔCBS of about 30 - 40 meV [56–59] where the optically bright exciton transition (X_0) is associated with the higher lying conduction band (the large splitting of the valence bands has been omitted for clarity). The chemical potential as estimated using the effective masses and band offsets in WS_2 monolayer from Ref. [56] is in the range of several 10's of meV for the typical doping conditions in our experiment (see Supplemental Material [44]). Thus, even at the highest doping density $8\cdot10^{12}$ cm^{-2}, more than 75 % of the electrons reside in the lower conduction band, so that the higher-lying band remains mostly unoccupied. As discussed below, this renders the WS_2 system particularly suitable to separate the screening phenomena from the Pauli-blocking effects in the relevant density regime.

In order to extract the evolution of the exciton binding energy and the quasi-particle band gap for different free carrier densities, we monitor the optically bright excited states of the exciton, in analogy to the analysis in the previous studies of excitons in as-exfoliated WS_2 [8] and WSe_2 [7]. In Fig. 2, we plot the second derivatives of the reflectance contrast for the undoped case (a,b) and at

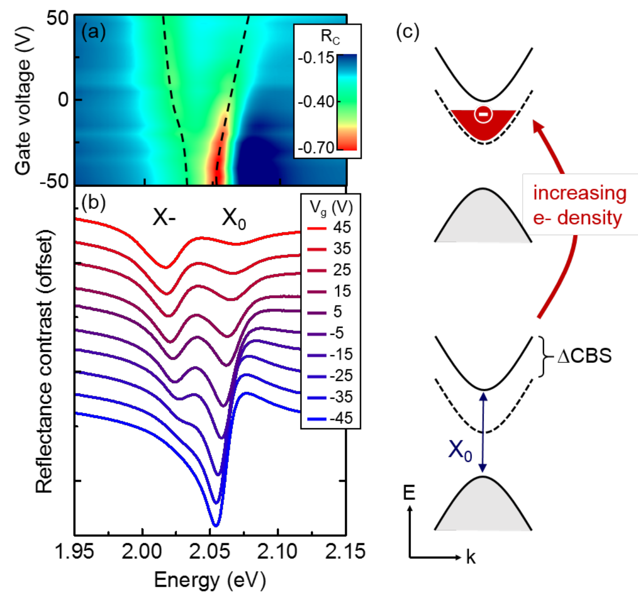

FIG. 1. (a) Color plot of the reflectance contrast (R_C) spectra for different gate voltages at a temperature of T = 50 K. Charge neutrality point is estimated to be around $V_g = -45$ V, and the estimated electron doping density scales roughly by $0.8\cdot10^{12}$ cm^{-2} per 10 V. The evolution of the charged and neutral exciton peaks is shown by dotted lines. (b) Reflectance contrast spectra for selected gate voltages, offset for clarity. (c) Schematic illustration of the relevant part of the WS_2 band structure around the fundamental band gap transition with (top) and without (bottom) electron doping. The spin-splitting of the conduction bands and the bright exciton transition are indicated by ΔCBS and X_0, respectively. The spin-split valence band lies much lower in energy and has been omitted for clarity.

the highest gate voltage (c,d) in the spectral range of the ground and excited state exciton resonances. The complete voltage series is shown in the Supplemental Material [44]. In addition to the exciton ground state and trion (Fig.2 (a,c)), we also observe weak features in the spectral range between 2.2 eV and 2.3 eV (Fig. 2 (b,d)). The later were identified in our previous work [8] as the first and second excited-state transitions of the exciton. The excitonic states, labeled according to their principal quantum number $n = 1, 2, 3$, exhibit shifts of their transition energies as the doping density is increased (Fig. 2 (c,d)). Signatures of higher excited states (n$>$3) are obscured by the noise in the present measurement. No spectral features associated with the excited states of the trion are observed, which is attributed to the absence of one-electron excited states for the negatively charged hydrogen-like state and the instability of the two-electron excited states due to efficient Auger-like auto-ionization [60].

Plotted in red and blue in Fig. 2 are the fitting functions used to extract the energy of the excited states. These curves correspond to the reflectance contrast spectra generated from the multi-Lorentzian parametriza-

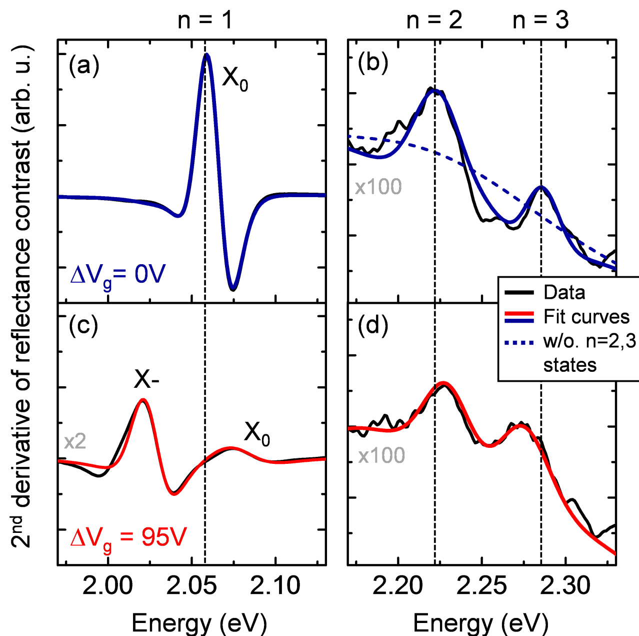

FIG. 2. Second derivatives of the reflectance contrast for gate voltages relative to the charge neutrality point of $\Delta V_g = 0\,\mathrm{V}$ (a,b) and ΔV_g=95 V (c,d), corresponding to the estimated electron doping density of about $8{\cdot}10^{12}\,\mathrm{cm}^{-2}$. Measured data are indicated by the black lines, and the results of the multi-Lorentzian model by red and blue curves. Both experimental and simulated curves are smoothed over a spectral range of 10 meV after each derivative is taken. The simulated curve without the $n = 2$ and $n = 3$ resonances is included in (b) for comparison.

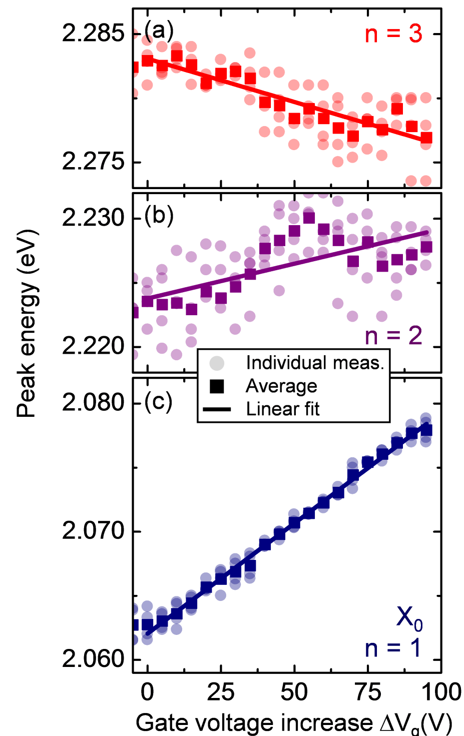

FIG. 3. Peak energies for the $n = 3$ (a), $n = 2$ (b), and $n = 1$ (c) exciton states as function of gate voltage ΔV_g relative to the charge neutrality point. The estimated electron doping density scales roughly by $0.8{\cdot}10^{12}\,\mathrm{cm}^{-2}$ per 10 V. Data from four individual measurements (light colored squares) at each gate voltage fare presented together with the respective averages (dark colored squares) and linear line fits (solid curves). The vertical scale of the energy axis is the same in all three plots.

tion of the dielectric function of the material, by taking into account the influence of the dielectric response of the underlying substrate. The parameters describing the excitonic features are adjusted to match the second derivatives of the experimental data. Also shown as dashed lines for comparison is the simulated curve without the $n = 2$ and $n = 3$ resonances. Figure 3 summarizes the extracted peak energies for the $n = 1, 2, 3$ exciton states as function of gate voltage ΔV_g relative to the charge neutrality point. At each gate voltage, the measurement is repeated four times, and the results are presented together with the respective average. The transition energies of the exciton states shift monotonically with the gate voltage. We use a simple linear relation to quantify the observed behavior, since the experimental uncertainty precludes the meaningful application of a more complex model. The corresponding solid lines in Fig. 3 are thus introduced to summarize the experimental trends and the monotonic evolution of the n=1,2,3 transitions. The corresponding slope parameters are $\Delta E_{n=1} = 0.172(\pm 0.0026)\,\mathrm{meV/V}$, $\Delta E_{n=2} = 0.054(\pm 0.013)\,\mathrm{meV/V}$, and $\Delta E_{n=3} = -0.067(\pm 0.007)\,\mathrm{meV/V}$.

Our observations can be considered to be the result both of the electrical doping of the sample and of the influence of the out-of-plane electric field (estimated to be below $2{\cdot}10^{-2}\,\mathrm{V\,Å}^{-1}$ for the maximum gate voltage of 50 V). As discussed in detail in Sect. 6 of the Supplemental Material [44], the influence of both the Stark effect and of the recently proposed "brightening" of the dark excitons [61] are negligible in comparison to the influence of gate-induced doping. In particular, the transfer of the oscillator strength from bright to dark states can be excluded as contributing significantly to our observations both because of the conduction band ordering in WS2 (with the dark state lying below the bright state) and because of the overall estimated strength of the effect. Thus, to interpret our findings we turn to the well-developed, many-body theory for quasi-2D semiconductors [62, 63], where the presence of the free charge carriers in the system is predicted to influence the measured optical spectra through three main physical mechanisms: elastic Coulomb scattering, Pauli blocking and screening of the Coulomb interaction. First, the scattering of excitons with free charge carriers leads to a de-

crease of the exciton coherence lifetime and thus to a spectral broadening of the exciton transitions. Second, Pauli-blocking typically induces a decrease of the exciton oscillator strength and binding energy due to the occupation of the electronic states and the fermionic nature of the electrons. Finally, the screening of the electric fields by the free charges reduces the overall strength of the Coulomb interaction. The screening of the *attractive* interaction between electrons and holes lowers the exciton oscillator strength and binding energy, similar to the effect of the Pauli blocking. Also, the exciton states with higher quantum numbers are affected more strongly due to their larger Bohr radii. The reduction of the *repulsive* interaction induces a decrease of the quasi-particle self-energy and thus leads to the renormalization of the band-gap to lower energies. The combined effect of the three contributions is summarized in Fig. 4(a), where the absorption spectra from an undoped and doped semiconductor are schematically indicated, including ground and excited exciton transitions, as well as the onset of the band gap. In the doped case, the band gap shifts to lower energies and the exciton peaks broaden and decrease in strength. The energy intervals between the exciton transitions and the band gap energy also decrease, reflecting the reduction of the respective binding energies. The absolute exciton transitions thus shift due to the combined effect from the reduced binding energies and band gap renormalization.

This scenario matches our experimental findings. Density-dependent broadening and the decrease of the overall oscillator strength of the exciton ground state are clearly observed (see Figs. 1 (a),(b) and Supplemental Material [44]). The shift of the excitonic states closer to one another in energy (Fig. 2) corresponds to the reduction of the exciton binding energy with increased gate voltage. Finally, the $n = 3$ transition shifts to lower energies following the decrease of the quasi-particle gap. We note that for low to intermediate carrier densities in 2D systems (that is, below the Mott transition from excitons to an electron-hole plasma), the contributions of Pauli blocking to the discussed phenomena is considered minor in comparison to that of screening [64]. In addition, as outlined above, Pauli blocking can be largely neglected for most experimental conditions in our study, since the upper conduction band in WS_2 monolayer is barely occupied. Therefore, the observed material response to doping is expected to be dominated by the Coulomb screening from the free electrons.

Within this framework, we can estimate the values for the binding energies and the quasi-particle band gap. Since the extracted shifts for the exciton peak energies are more reliable than the absolute values due to the experimental uncertainty, we fix the band gap and the $n = 1$ binding energy to the previously determined values of 2.4 eV and 320 meV, respectively [8]. The doping conditions for the sample studied in the Ref. [8] correspond to $\Delta V_g = 35\,$V, as determined from the neutral and charged exciton peak energies (see Supplemental Material [44]). In addition, the absolute peak energies of the exciton peaks of $E_{n=1} = 2.07\,$eV, $E_{n=2} = 2.23\,$eV, and $E_{n=3} = 2.28\,$eV compare well with the corresponding values from Ref. [8] of 2.09 eV, 2.23 eV, and 2.31 eV. The respective binding energies are represented by circles in Fig. 4 (b). We use two basic assumptions to estimate the minimum and maximum shifts of the band gap. On the one hand, the minimum band gap shift is determined by the condition that the relative change of the $n = 3$ binding energy has to be larger than the relative change of the $n = 2$ binding energy for all doping densities. On the other hand, the maximum band gap shift is determined by the observation of the $n = 3$ peak even at the highest doping level, so that the band gap position has to be higher in energy by at least half of the line width of the $n = 3$ transition. The resulting estimates for the band gap energy are presented in Fig. 4 (c) and the evolution of the corresponding exciton binding energies is shown in Fig. 4 (b), where the experimental data is represented by the linear fits.

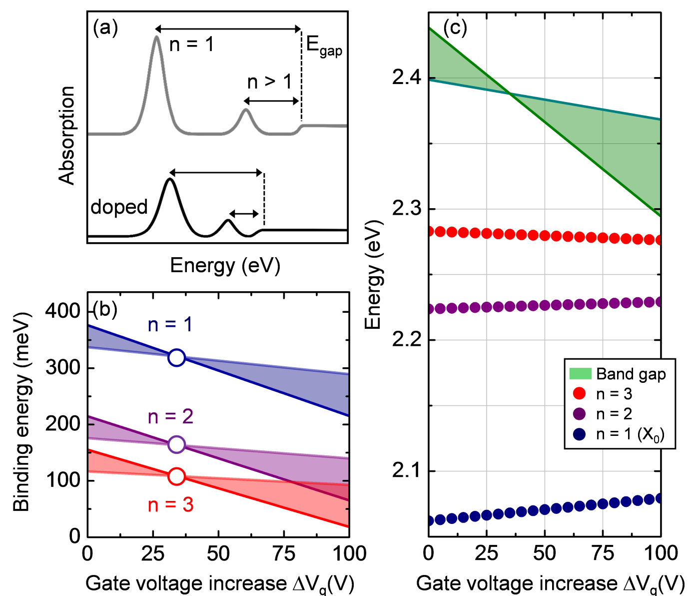

FIG. 4. (a) Schematic illustration of the absorption spectra for an undoped (top) and doped (bottom) 2D semiconductor. The quasi-particle band gap position E_{gap} is represented by the dashed line, and the ground and excited exciton states are indicated by $n = 1$ and $n > 1$, respectively. (b) Evolution of the exciton binding energies as function of the relative gate voltage ΔV_g as estimated from the minimum and maximum shifts of the band gap. The estimated electron doping density scales roughly by $0.8{\cdot}10^{12}\,\mathrm{cm}^{-2}$ per 10 V. Values for the exciton binding energies at $\Delta V_g = 35\,$V are fixed from Ref. [8] and are represented by circles. (c) Absolute energies of the $n = 1, 2, 3$ exciton states and the estimated minimum and maximum shifts of the band gap. Linear fits to the experimental data are used in (b) and (c) for clarity.

On average, the screening of the Coulomb interaction induces a band gap shift on the order of 100 ($\pm$60) meV and a comparable change in the binding energy of the exciton ground state at the highest doping density of about $8{\cdot}10^{12}$ electrons cm^{-2}. Extrapolating the evolution of binding energies to even higher doping densities results in the complete screening of the $n=1$, $n=2$, and $n=3$ states at the electron densities of $3.7\,(\pm1.9){\cdot}10^{13}\,\mathrm{cm}^{-2}$, $2.8\,(\pm1.7){\cdot}10^{13}\,\mathrm{cm}^{-2}$, and $2.4\,(\pm1.5){\cdot}10^{13}\,\mathrm{cm}^{-2}$. In particular, the ionization of the exciton ground state ($n=1$) corresponds to the threshold for the Mott transition from the excitonic to electron-hole plasma regime. We note, however, that these values should be considered as rough estimates due to the linear extrapolation.

In summary, we have demonstrated the continuous, electrical tuning of the exciton binding energy in a monolayer WS_2 integrated into a FET device. The evolution of the exciton properties with the gate voltage is monitored by tracking the optical signatures of the excited exciton states ($n=1,2,3$) via reflectance spectroscopy. By changing the voltage from -50 V to +50 V both the exciton binding energy and the quasi-particle band-gap position are tuned across the energy range of about 100 meV. The observed phenomena are associated with the electrical injection of free charge carriers into the WS_2 monolayer at densities up to $8{\cdot}10^{12}\,\mathrm{cm}^{-2}$. The resulting decrease of the exciton binding energies and the renormalized band-gap position are mainly attributed to the screening of the Coulomb interaction by the free charges. The complete ionization of the excitons is estimated to occur at a carrier density of several $10^{13}\,\mathrm{cm}^{-2}$.

[1] K. S. Novoselov, D. Jiang, F. Schedin, T. J. Booth, V. V. Khotkevich, S. V. Morozov, and A. K. Geim, Proc. Natl. Acad. Sci. USA **102**, 10451 (2005).
[2] A. Splendiani, L. Sun, Y. Zhang, T. Li, J. Kim, C.-Y. Chim, G. Galli, and F. Wang, Nano Lett. **10**, 1271 (2010).
[3] K. F. Mak, C. Lee, J. Hone, J. Shan, and T. F. Heinz, Phys. Rev. Lett. **105**, 136805 (2010).
[4] L. Brus, Acc. Chem. Res. **47**, 2951 (2014).
[5] F. Xia, H. Wang, D. Xiao, M. Dubey, and A. Ramasubramaniam, Nat. Photon. **8**, 899 (2014).
[6] C. Zhang, A. Johnson, C.-L. Hsu, L.-J. Li, and C.-K. Shih, Nano Lett. **14**, 2443 (2014).
[7] K. He, N. Kumar, L. Zhao, Z. Wang, K. F. Mak, H. Zhao, and J. Shan, Phys. Rev. Lett. **113**, 026803 (2014).
[8] A. Chernikov, T. C. Berkelbach, H. M. Hill, A. Rigosi, Y. Li, O. B. Aslan, D. R. Reichman, M. S. Hybertsen, and T. F. Heinz, Phys. Rev. Lett. **113**, 076802 (2014).
[9] Z. Ye, T. Cao, K. O'Brien, H. Zhu, X. Yin, Y. Wang, S. G. Louie, and X. Zhang, Nature **513**, 214 (2014).
[10] M. M. Ugeda, A. J. Bradley, S.-F. Shi, F. H. da Jornada, Y. Zhang, D. Y. Qiu, S.-k. Mo, Z. Hussain, Z.-X. Shen, F. Wang, S. G. Louie, and M. F. Crommie, Nat. Mater. **13**, 1091 (2014).
[11] K. F. Mak, K. He, C. Lee, G. H. Lee, J. Hone, T. F. Heinz, and J. Shan, Nat. Mater. **12**, 207 (2013).
[12] J. S. Ross, S. Wu, H. Yu, N. J. Ghimire, A. M. Jones, G. Aivazian, J. Yan, D. G. Mandrus, D. Xiao, W. Yao, and X. Xu, Nat. Commun. **4**, 1474 (2013).
[13] Y. You, X. Zhang, T. C. Berkelbach, M. S. Hybertsen, D. R. Reichman, and T. F. Heinz, Nat. Phys. **11**, 477 (2015).
[14] T. Cheiwchanchamnangij and W. R. L. Lambrecht, Phys. Rev. B **85**, 205302 (2012).
[15] A. Ramasubramaniam, Phys. Rev. B **86**, 115409 (2012).
[16] H.-P. Komsa and A. V. Krasheninnikov, J. Phys. Chem. Lett. **3**, 3652 (2012).
[17] H. Shi, H. Pan, Y.-W. Zhang, and B. I. Yakobson, Phys. Rev. B **87**, 155304 (2013).
[18] A. Molina-Sánchez, D. Sangalli, K. Hummer, A. Marini, and L. Wirtz, Phys. Rev. B **88**, 045412 (2013).
[19] D. Y. Qiu, F. H. da Jornada, and S. G. Louie, Phys. Rev. Lett. **111**, 216805 (2013).
[20] F. Hüser, T. Olsen, and K. S. Thygesen, Phys. Rev. B **88**, 245309 (2013).
[21] T. C. Berkelbach, M. S. Hybertsen, and D. R. Reichman, Phys. Rev. B **88**, 045318 (2013).
[22] C. Zhang, H. Wang, W. Chan, C. Manolatou, and F. Rana, Phys. Rev. B **89**, 205436 (2014).
[23] G. Berghäuser and E. Malic, Phys. Rev. B **89**, 125309 (2014).
[24] A. Steinhoff, M. Rösner, F. Jahnke, T. O. Wehling, and C. Gies, Nano Lett. **14**, 3743 (2014).
[25] H. M. Hill, A. F. Rigosi, C. Roquelet, A. Chernikov, T. C. Berkelbach, D. R. Reichman, M. S. Hybertsen, L. E. Brus, and T. F. Heinz, Nano Lett. **15**, 2992 (2015).
[26] Y. Li, A. Chernikov, X. Zhang, A. Rigosi, H. M. Hill, A. M. van der Zande, D. A. Chenet, E.-M. Shih, J. Hone, and T. F. Heinz, Phys. Rev. B **90**, 205422 (2014).
[27] X. Liu, T. Galfsky, Z. Sun, F. Xia, E.-c. Lin, Y.-H. Lee, S. Kéna-Cohen, and V. M. Menon, Nat. Photon. **9**, 30 (2014).
[28] C. Poellmann, P. Steinleitner, U. Leierseder, P. Nagler, G. Plechinger, M. Porer, R. Bratschitsch, C. Schüller, T. Korn, and R. Huber, Nat. Mater. , doi:10.1038/nmat4356 (2015).
[29] G. Eda, H. Yamaguchi, D. Voiry, T. Fujita, M. Chen, and M. Chhowalla, Nano Lett. **11**, 5111 (2011).
[30] P. Tonndorf, R. Schmidt, P. Böttger, X. Zhang, J. Börner, A. Liebig, M. Albrecht, C. Kloc, O. Gordan, D. R. T. Zahn, S. Michaelis de Vasconcellos, and R. Bratschitsch, Opt. Express **21**, 4908 (2013).
[31] N. Scheuschner, O. Ochedowski, A.-M. Kaulitz, R. Gillen, M. Schleberger, and J. Maultzsch, Phys. Rev. B **89**, 125406 (2014).
[32] K. F. Mak, K. He, J. Shan, and T. F. Heinz, Nat. Nanotechnol. **7**, 494 (2012).
[33] D. Xiao, G.-B. Liu, W. Feng, X. Xu, and W. Yao, Phys. Rev. Lett. **108**, 196802 (2012).
[34] H. Zeng, B. Zhu, K. Liu, J. Fan, X. Cui, and Q. M. Zhang, Phys. Rev. B **86**, 241301 (2012).
[35] T. Cao, G. Wang, W. Han, H. Ye, C. Zhu, J. Shi, Q. Niu, P. Tan, E. Wang, B. Liu, and J. Feng, Nat. Commun. **3**, 887 (2012).
[36] A. M. Jones, H. Yu, N. J. Ghimire, S. Wu, G. Aivazian, J. S. Ross, B. Zhao, J. Yan, D. G. Mandrus, D. Xiao, W. Yao, and X. Xu, Nat. Nanotechnol. **8**, 634 (2013).
[37] K. F. Mak, K. L. McGill, J. Park, and P. L. McEuen,

Science **344**, 1489 (2014).
[38] D. Lagarde, L. Bouet, X. Marie, C. R. Zhu, B. L. Liu, T. Amand, P. H. Tan, and B. Urbaszek, Phys. Rev. Lett. **112**, 047401 (2014).
[39] J. Kim, X. Hong, C. Jin, S.-F. Shi, C.-Y. S. Chang, M.-H. Chiu, L.-J. Li, and F. Wang, Science **346**, 1205 (2014).
[40] D. MacNeill, C. Heikes, K. F. Mak, Z. Anderson, A. Kormányos, V. Zólyomi, J. Park, and D. C. Ralph, Phys. Rev. Lett. **114**, 037401 (2015).
[41] G. Aivazian, Z. Gong, a. M. Jones, R. L. Chu, J. Yan, D. G. Mandrus, C. Zhang, D. Cobden, W. Yao, and X. D. Xu, Nat. Phys. **11**, 148 (2015).
[42] A. Srivastava, M. Sidler, A. V. Allain, D. S. Lembke, A. Kis, and A. Imamoglu, Nat. Phys. **11**, 141 (2015).
[43] E. J. Sie, J. W. McIver, Y.-H. Lee, L. Fu, J. Kong, and N. Gedik, Nat. Mater. **14**, 290 (2015).
[44] See Supplemental Material at [url], which includes Refs. [45-52].
[45] G. V. Astakhov, V. P. Kochereshko, D. R. Yakovlev, W. Ossau, J. Nürnberger, W. Faschinger, and G. Landwehr, Phys. Rev. B **62**, 10345 (2000).
[46] A. Esser, E. Runge, R. Zimmermann, and W. Langbein, Phys. Stat. Sol. (a) **178**, 489 (2000).
[47] S. W. Koch, T. Meier, F. Jahnke, and P. Thomas, Appl. Phys. A **71**, 511 (2000).
[48] H. Wang, K. Ferrio, D. Steel, Y. Hu, R. Binder, and S. W. Koch, Phys. Rev. Lett. **71**, 1261 (1993).
[49] C. Klingshirn, *Semiconductor Optics*, 3rd ed. (Springer, Berlin Heidelberg New York, 2007).
[50] D. A. B. Miller, D. S. Chemla, T. C. Damen, A. C. Gossard, W. Wiegmann, T. H. Wood, and C. A. Burrus, Phys. Rev. Lett. **53**, 2173 (1984).
[51] J. Singh, Appl. Phys. Lett. **64**, 2694 (1994).
[52] J. Kang, S. Tongay, J. Zhou, J. Li, and J. Wu, Appl. Phys. Lett. **102**, 012111 (2013).
[53] A. A. Mitioglu, P. Plochocka, J. N. Jadczak, W. Escoffier, G. L. J. A. Rikken, L. Kulyuk, and D. K. Maude, Phys. Rev. B **88**, 245403 (2013).
[54] A. Singh, G. Moody, S. Wu, Y. Wu, N. J. Ghimire, J. Yan, D. G. Mandrus, X. Xu, and X. Li, Phys. Rev. Lett. **112**, 216804 (2014).
[55] G. Plechinger, P. Nagler, J. Kraus, N. Paradiso, C. Strunk, C. Schüller, and T. Korn, Phys. Stat. Sol. RRL , doi:10.1002/pssr.201510224 (2015).
[56] G. B. Liu, W. Y. Shan, Y. Yao, W. Yao, and D. Xiao, Phys. Rev. B **88**, 085433 (2013).
[57] K. Kośmider and J. Fernández-Rossier, Phys. Rev. B **87**, 075451 (2013).
[58] A. Kormányos, V. Zólyomi, N. D. Drummond, and G. Burkard, Phys. Rev. X **4**, 011034 (2014).
[59] A. Kormányos, G. Burkard, M. Gmitra, J. Fabian, V. Zólyomi, N. D. Drummond, and V. Fal'ko, 2D Mater. **2**, 022001 (2015).
[60] A. R. P. Rau, J. Astrophys. Astr. **17**, 113 (1996).
[61] H. Dery and Y. Song, (2015), arXiv:1506.06686.
[62] N. Peyghambarian, S. W. Koch, and A. Mysyrowicz, *Introduction to semiconductor optics* (Prentice-Hall, Inc., 1993).
[63] H. Haug and S. W. Koch, *Quantum theory of the optical and electronic properties of semiconductors*, 5th ed. (World Scientific, Singapore, 2009).
[64] S. Nojima, Phys. Rev. B **51**, 11124 (1995).

ACKNOWLEDGMENTS

The authors would like to thank Timothy C. Berkelbach, Mark S. Hybertsen, and David R. Reichman for fruitful discussions. This work was supported by the U.S. Department of Energy, Office of Science, Office of Basic Energy Sciences, with funding at Columbia University through the Energy Frontier Research Center under grant DE-SC0001085 for optical measurements and at SLAC National Accelerator Laboratory through the AMOS program within the Chemical Sciences, Geosciences, and Biosciences Division for data analysis. Device fabrication was supported by the Nanoelectronics and Beyond program of the National Science Foundation (grant DMR-1124894) and the Nanoelectronics Research Initiative of the Semiconductor Research Corporation. A.C. gratefully acknowledges funding from the Alexander von Humboldt Foundation within the Feodor Lynen Research Fellowship program and from the Keck Foundation. H. M. H. and A. F. R. were supported, respectively, by the NSF through an IGERT Fellowship (grant DGE-1069240) and through a Graduate Research Fellowship (grant DGE-1144155).